GEOPHYSICAL RESEARCH LETTERS, VOL. 35, L01608, doi:10.1029/2007GL032100, 2008

Cyclonic and anticyclonic motion in the upper ocean

Annalisa Griffa,[1,2] Rick Lumpkin,[3] and Milena Veneziani[4]

Received 20 September 2007; accepted 9 November 2007; published 15 January 2008.

[1] Upper ocean variability is highly energetic and contributes to key processes such as heat transport and water mass formation. Here, the distribution of ocean surface cyclonic and anticyclonic motion is computed from global drifter observations for scales from large eddies to submesoscale. Two zonal bands of small-scale motion are recovered: a known anticyclonic band at 30°–40° latitude, mostly wind-induced, and an unexpected cyclonic band at 10°–20° latitude. It is suggested that this is due to submesoscale processes related to salinity front instabilities. These results provide a first global view of the upper ocean including these motions. **Citation:** Griffa, A., R. Lumpkin, and M. Veneziani (2008), Cyclonic and anticyclonic motion in the upper ocean, *Geophys. Res. Lett.*, *35*, L01608, doi:10.1029/2007GL032100.

1. Introduction and Motivation

[2] The upper ocean plays a fundamental role in the set up of both wind driven and thermohaline circulation. Despite this importance, many aspects of upper ocean dynamics are still unknown, especially how its variability is characterized by the interaction of different types of motion and scales. Upper ocean variability is characterized by coherent eddies, mostly geostrophic and generated by instabilities, and by ageostrophic motion related to direct wind action in the Ekman layer and to submesoscale dynamics at scales smaller than the Rossby deformation radius [*Chelton et al.*, 1998].

[3] In this paper, we investigate the properties of upper ocean variability using global surface drifter data [*Sybrandy and Niiler*, 1991], focusing on the distribution of polarity and investigating the nature of the motions that determine this distribution. The analysis is performed in the subtropical and subpolar regions (10°–60° latitude), which are well sampled by the drifters, and is focused on the subinertial but relatively high frequency motion characterized by periods of ≈5–20 days. The results allow us to identify the contribution of various scales of motion, from large and mesoscale eddies to smaller scale structures, providing new insights into the role of submesoscale motion. In particular, an unexpected and well defined zonal band of cyclonic submesoscale motion previously undetected is revealed around 10°–20° latitude in all ocean basins.

2. Methodology

2.1. General Description

[4] The spin Ω [*Borgas et al.*, 1997], first introduced in the framework of Lagrangian stochastic models and recently applied to subsurface ocean floats [*Veneziani et al.*, 2004, 2005a], describes the mean rotation per time interval computed along a trajectory, $\Omega = \langle u' \, dv' - v' \, du' \rangle / (2\Delta t \, \mathrm{EKE})$, where u' and v' are the components of the Lagrangian residual velocity computed with respect to the mean flow $\mathbf{U}_s$ (section 2.2), Δt is the time sampling interval, and EKE is the eddy kinetic energy, $0.5 \langle u'^2 + v'^2 \rangle$. Trajectories with nonzero spin are associated with looping or spiraling motion, and are referred to as "loopers" [*Richardson*, 1993]. Particles with zero spin, on the other hand, move as in a random walk. Loopers are often identified with coherent eddies [*Richardson*, 1993], but can also be due to direct wind forcing or waves, such as Rossby waves [*Flierl*, 1981], inertial, tidal or equatorial waves. As our study is focused on subinertial and nonequatorial motion, inertial and equatorial waves are not expected to play a significant role, but Rossby waves and Ekman dynamics can be relevant. For loopers in the core of a coherent eddy, Ω is a good approximation of (half) the relative vorticity, ζ, $\zeta \sim 2\Omega$ [*Veneziani et al.*, 2005a]. For all loopers, Ω provides direct information on particle rotation and polarity [*Veneziani et al.*, 2004, 2005b], with positive (negative) Ω associated with cyclonic (anticyclonic) motion in the Northern hemisphere (opposite sign in the Southern hemisphere).

[5] In previous regional investigations [*Richardson*, 1993], loopers were identified by visual inspection, but this method is unsuitable for global applications. Here we use an automated method [*Veneziani et al.*, 2004, 2005b; *Doglioli et al.*, 2006] that identifies loopers as trajectories with an average value of spin greater than a cut-off value Ω_c (section 2.2).

2.2. Data Analysis

[6] The data set consists of the trajectories of standardized drifters drogued at a depth of 15 m to follow near-surface ocean currents (data available at http://www.aoml.noaa.gov/phod/dac/gdp_drifter.html). Undrogued drifters and those operating at a duty cycle of 1/2 or less were excluded. Velocities $\mathbf{u}(\mathbf{x}, t)$ were calculated from 6-hourly interpolated positions via a 12 h centered difference.

[7] Seasonal mean currents $\mathbf{U}_s(\mathbf{x}, t)$ [*Lumpkin and Garraffo*, 2005] were calculated globally at a resolution of 1° and mapped via 2D linear interpolation to each 6 h drifter location. Residual velocities were calculated as $\mathbf{u}' = \mathbf{u} - \mathbf{U}_s$. Since we are interested in subinertial motion, inertial motion has been filtered out by dividing the drifter trajectories into

[1]Istituto de Scienze Marine, Consiglio Nazionale delle Ricerche, Pozzuolo di Lerici, Italy.
[2]Also at Division of Meteorology and Physical Oceanography, Rosenstiel School of Marine and Atmospheric Science, University of Miami, Miami, Florida, USA.
[3]Physical Oceanography Division, NOAA Atlantic Oceanographic and Meteorological Laboratory, Miami, Florida, USA.
[4]Ocean Sciences Department, University of California, Santa Cruz, California, USA.

0094-8276/08/2007GL032100$05.00

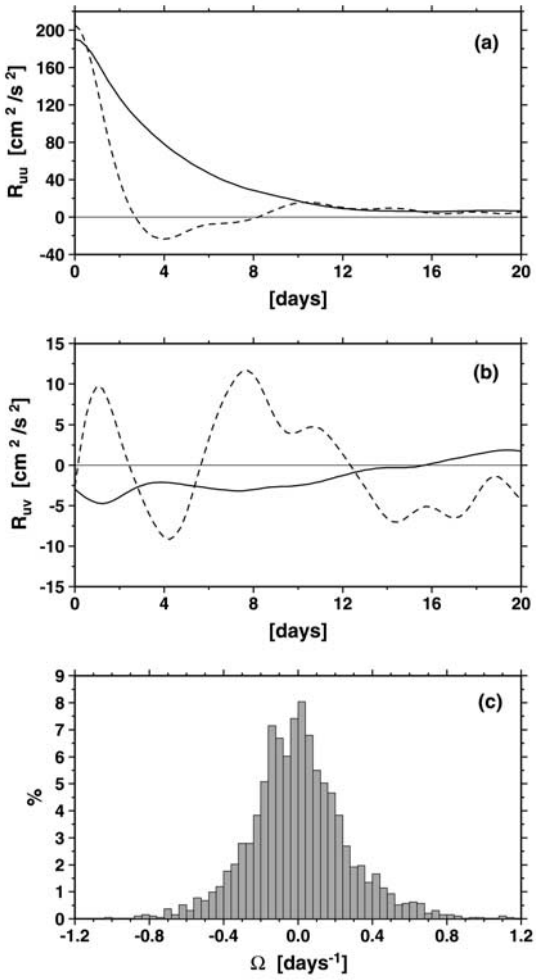

Figure 1. (a) Autocovariance and (b) crosscovariance functions of the zonal Lagrangian velocity (similar figures hold for the meridional velocity) in the subtropical North Atlantic (18–32°N, 30–72.5°W). Two different regimes are shown, corresponding to trajectories with high spin values ($|\Omega| > \Omega_c = 0.4$ day^{-1}, dashed lines), and low spin values ($|\Omega| < \Omega_c$, solid lines). (c) Probability density function of spin values Ω averaged over trajectory segments of length $T_{seg} = 20$ days.

non-overlapping segments of length T_{seg}, identifying the inertial period IP from the median latitude of each segment, and lowpassing the residual velocity to remove motion with period smaller than 1.5 IP. Inspection of rotary spectra confirmed that the inertial energy was reduced by many orders of magnitude and that filter leakage did not influence other frequency content.

[8] The resulting data set consists of 3922 drifter-years of velocity measurements, spanning the time period 1992–2006, with high spatial coverage (Figure S1 of the auxiliary material)[1] up to subpolar latitudes (~60°). This paper focuses on the subtropical and subpolar regions (10°–60°), excluding the poorly covered polar areas and the heavily filtered equatorial band.

[1]Auxiliary materials are available in the HTML. doi:10.1029/2007GL032100.

[9] For each trajectory segment T_{seg}, the average value of spin Ω was computed, and a cut off value Ω_c was determined to distinguish between loopers and nonloopers. To identify the values of the parameters T_{seg} and Ω_c, an extensive preliminary sensitivity analysis was performed in four representative regions of the North Atlantic: north and south of the Gulf Stream extension (39°–48°N, 52°–70°W; 33°–37°N, 49°–71°W), part of the subpolar gyre (52°–60°N, 30°–70°W), and in the subtropical region (18°–32°N, 30°–72.5°W). Results show that, despite the dynamically different characteristics of the regions, appropriate values of T_{seg} and Ω_c remain relatively constant. In all cases, the results appear only weakly sensitive to T_{seg} in the range $T_{seg} = 20$–40 days, while an appropriate value for Ω_c is ~0.4 day^{-1} in all regions. An example of results in the subtropical region separating loopers and nonloopers using $T_{seg} = 20$ days and $\Omega_c = 0.4$ day^{-1} is shown in Figure 1. The statistical properties of the looper/nonlooper trajectories are markedly different, with the loopers exhibiting a negative lobe in the velocity autocovariance (Figure 1a) and well defined oscillations in the crosscovariance (Figure 1b), both indicative of rotational motion, while the nonloopers exhibit an exponentially decaying autocovariance and a flatter crosscovariance. Also, the probability density function (pdf) of the spin values computed for each trajectory segment (Figure 1c) shows a clear deviation from Gaussianity, with skewness 0.49 ± 0.21, indicating an extended cyclonic tail, and kurtosis 1.50 ± 0.39, e.g., extreme values are significantly more likely than in a purely Gaussian pdf. Results in the other regions are qualitatively similar, although the pdf's appear more complex in the region south of the Gulf Stream, likely because of superposition of various energetic motions.

3. Results

[10] The global mean polarity distribution is shown in Figure 2 (left), computed as the average of all spin values (sign reversed for the Southern hemisphere) in 5° × 5° bins. While the effects of large scale fronts associated with the major currents can be recognized, the most striking aspect is the large-scale zonal pattern, with two bands of alternated polarity: an anticyclonic band around 30°–40° N and S (less evident in the North Atlantic), and a cyclonic band around 10°–20° N and S in the Atlantic, Pacific and South Indian Oceans (with variations in the specific latitude depending on the ocean). This large scale pattern can be seen in the global zonally averaged distribution (Figure 2, right), with the anticyclonic band enhanced in the Southern hemisphere most likely because of Agulhas rings (as suggested also by the results in Figure 3, bottom, and Figure 4, bottom). The presence of an anticyclonic band has been previously noticed in drifter rotary spectra [*Rio and Hernandez*, 2003; *Elipot*, 2006], while the cyclonic band has not been detected before to the authors' knowledge.

[11] In order to better understand the types of motion responsible for Figure 2, looper ($\Omega > \Omega_c$) trajectories of length T_{seg} were isolated for analysis. These trajectories' mean position and root mean square velocity u_{rms} (from the residual velocities u′) were calculated, as were the rotational time scale $T = 2\pi/\Omega$ and radial space scale $R = u_{rms}/\Omega$. A sensitivity analysis was performed by varying the values of

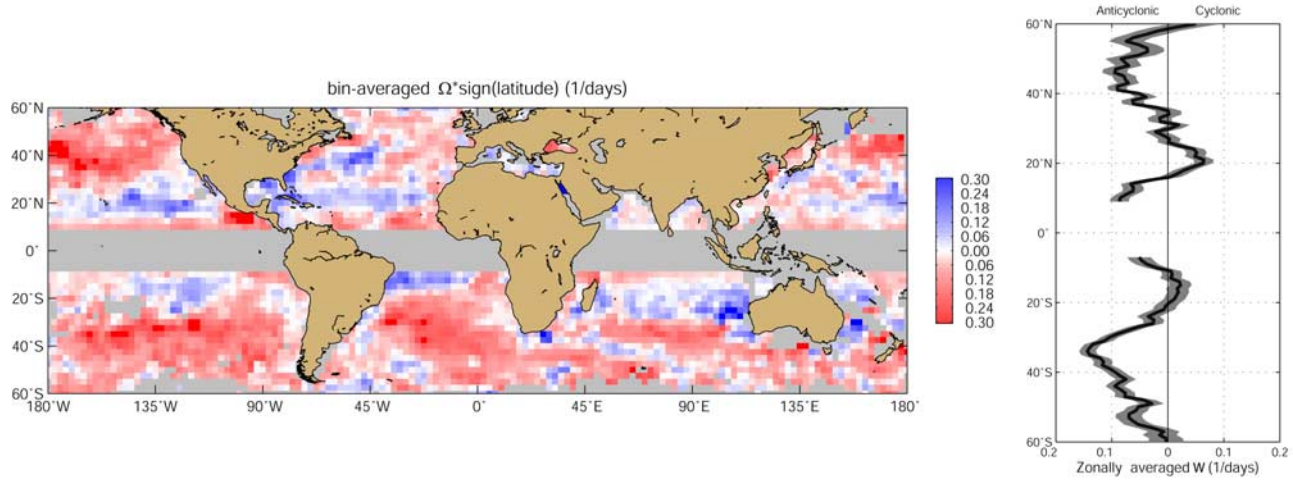

Figure 2. (left) 5° × 5° bin averaged distribution of spin (day^{-1}, with sign reversed in the Southern hemisphere): cyclones (anticyclones) are indicated by blue, positive values (red, negative values). (right) Zonally averaged distribution.

the parameters, and the resulting patterns were robust at varying T_{seg} (20, 40 days) and Ω_c (0.4, 0.5, 0.6 day^{-1}) (see Figure S2 of the auxiliary material). For $\Omega_c = 0.5$ day^{-1} and $T_{seg} = 20$ days, the polarity and R distributions are shown in Figure 3. The T distribution is not shown because it does not have a significant pattern, simply indicating a mixture of values in the range T ∼ 5–15 days at all latitudes.

[12] The looper polarity distribution (Figure 3, top) is consistent with the average distribution (Figure 2, left) indicating that loopers are responsible for the observed patterns. Further information about the specific motions and their scales can be gained from the R distribution (Figure 3, bottom). Large eddies and rings [*Olson*, 1991] appear as maximum values of R (≈60–120 km) and u_{rms}

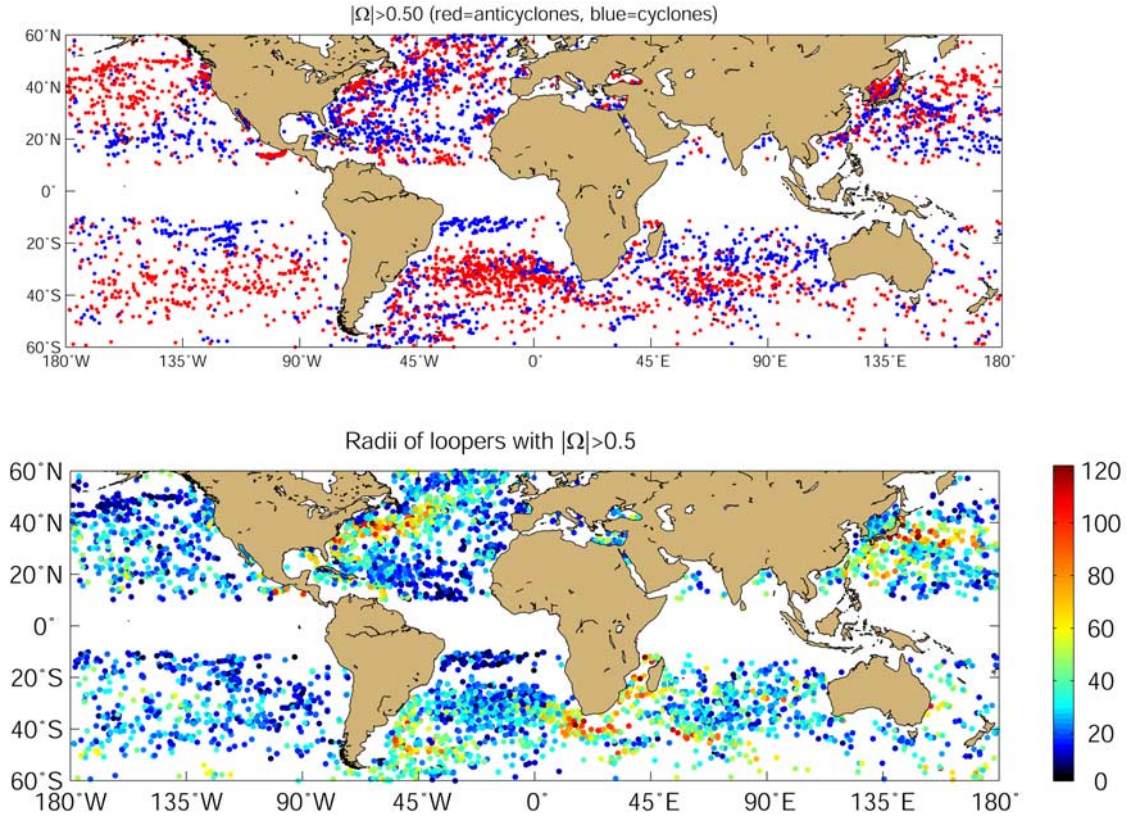

Figure 3. Distribution of individual trajectories with defined sense of rotation (spin values $|\Omega| > \Omega_c$). Each dot corresponds to the medial position of a trajectory segment of length $T_{seg} = 20$ days and $|\Omega| > \Omega_c = 0.5$ day^{-1}. Similar results are obtained for $T_{seg} = 40$ days and $\Omega_c = 0.4–0.6$ day^{-1} (not shown). (top) Distribution of polarity; cyclonic (blue) and anticyclonic (red). (bottom) Distribution of radial space scale $R = u_{rms}/\Omega$ (km).

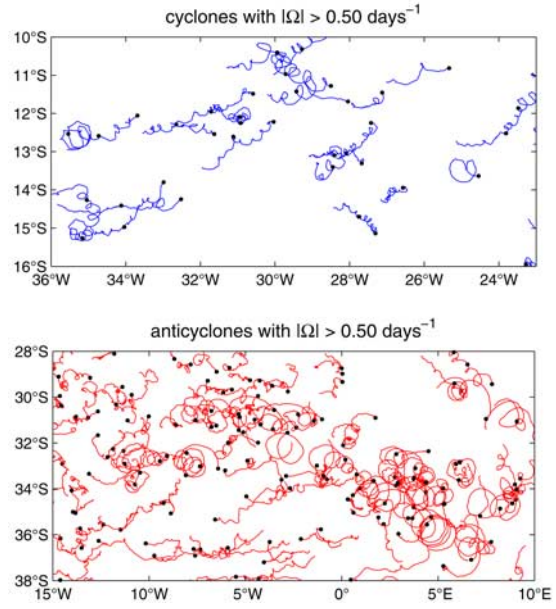

Figure 4. Examples of individual trajectory segments (T_{seg} = 20 days) with defined sense of rotation (spin values $|\Omega| > \Omega_c$) in the South Atlantic Ocean. (top) Cyclones. (bottom) Anticyclones. The black dots indicate the starting location of each trajectory segment.

(≈40–60 cm/s) (Figure S3 of the auxiliary material). They include cyclonic (anticyclonic) rings south (north) of the Gulf Stream and Kuroshio jets, anticyclonic Agulhas rings and cyclones penetrating the South Atlantic Ocean west of South Africa, and anticyclonic and cyclonic eddies in the Mozambique Channel and the Brazil-Malvinas confluence. The signature of smaller, less energetic mesoscale eddies is also seen, mostly related to baroclinic instabilities. They include eddies at relatively low latitude, around 20° in the North Pacific Subtropical Current and in the Southern Indian Ocean with R ≈ 50–60 km, and at higher latitudes, in the Japan Sea, Azores front and Gulf of Alaska with R ≈ 30–40 km. The latitudinal decrease in R is in qualitative agreement with the decrease of the Rossby radius of deformation [*Chelton et al.*, 1998]. A number of significantly smaller structures, with R ≈ 10–20 km and u_{rms} ≈ 10–20 cm/s, can also be identified, predominantly in the two latitudinal bands. These bands are not apparent when R < 30 km values are excluded from the distribution (not shown) except for the westward-equatorward intrusion of Agulhas rings in the South Atlantic. This type of motion (evident also in Figure 4, bottom) is consistent with nonlinear Rossby wave drift, as described by *Chelton et al.* [2007].

[13] The high and low spin trajectories can be visually examined to gain a more direct representation of the small-scale structures. Typical examples of raw trajectories (i.e. before filtering and demeaning) in the two polarity bands are shown in Figure 4 for the case of the South Atlantic. The cyclones (Figure 4, top) are characterized by trajectories with tight loops or cusps with small radii, mostly in the range of 10–20 km, in agreement with the R estimate in Figure 3 (bottom). The looping appears coherent for relatively long times, up to 60 days for some of the trajectories. The small anticyclonic structures appear more variable, less organized and with fewer loops than the cyclones. In the South Atlantic band (Figure 4, bottom), small anticyclones can be seen together with organized Agulhas rings propagating westward. At higher latitudes (>40°) the trajectories show a more meandering pattern. The spin method does not differentiate closed loops from meanders in the presence of strong mean currents when the meanders have significant rotation.

4. Discussion

[14] What is the generation mechanism of these small-scale bands? For the anticyclonic band, cross-spectral analysis [*Rio and Hernandez*, 2003] has shown significant coherence between drifter velocity and the wind, which itself has anticyclonic polarity. Coherences are not high (typically below 0.5), but they show maxima in the same areas where we see the highest concentration of small-scale features, i.e. in the Gulf of Alaska and the southern South Atlantic and Pacific oceans. These results suggest that the small-scale anticyclonic loopers are related to the upper ocean Ekman response to the wind. *Tomczak et al.* [2004] suggests a possible interplay between wind-driven and mixed layer frontal dynamics. *Elipot* [2006] notes that in the framework of time-dependent Ekman dynamics there is a preferential anticyclonic response to the wind also at subinertial frequencies, shown by the analysis of both drifter data and Ekman layer models.

[15] For cyclonic motion, the coherence with the wind is significantly smaller than it is for anticyclonic motion, and no definite wind polarity has been detected [*Rio and Hernandez*, 2003]. Also the persistence of the looping trajectories (Figure 4, top) does not suggest Ekman dynamics. Rather, the looper characteristics appear consistent with trapping in propagating submesoscale vortices (SMVs). The location of the bands, roughly corresponding to the equatorward side of the subtropical gyres, is characterized by the presence of the surface Salinity Subtropical Front and coincides very closely with regions of subtropical Barrier Layer (BL) formation [*Sato et al.*, 2006], i.e., bottom mixed layer waters characterized by high salinity and homogeneous temperature. Synoptic BLs show a patchy distribution suggestive of episodic formation and propagation, linked to subduction or convection occurring at sharp, small-scale salinity fronts [*Sato et al.*, 2006]. The SMVs may be related to these frontal instabilities, playing a role in BL water formation.

[16] But why should surface SMVs be mostly cyclonic? Cyclonic prevalence in upper ocean submesoscale structures has been suggested by theoretical considerations of potential vorticity conservation at high Rossby number [*Hoskins and Bretherton*, 1972], confirmed from recent numerical simulations [*Boccaletti et al.*, 2007], and supported by satellite photographs of cyclonic spiral eddies [*Munk et al.*, 2000] and high-resolution current data in the North Pacific [*Rudnick*, 2001]. Our results provide a new and more global view, which confirms the cyclonic prevalence of submesoscale motion, while also raising a question about why cyclonic submesoscale eddies should be predominantly seen in the 10°–20° latitudinal band. Perhaps, since the band is relatively quiescent without strong mesoscale activity or prevalent wind forcing variability, SMVs

can more easily be detected, or the dynamics of the band may be more conducive to SMV formation. Several hypotheses can be made. The scales of SM instabilities are set by the mixed-layer deformation radius [*Boccaletti et al.*, 2007] and can significantly decrease with latitude (although the deepening of the mixed layer at high latitude might counteract this effect). If the scales become too small, SMVs might not be detected or filtered out. Also, SMVs at high latitude might have significantly shorter lifetime because of more frequent occurrence of storms, and therefore be harder to detect over a T_{seg} period. Finally, even assuming fixed scales at different latitudes, the Rossby number is expected to increase at low latitude, which could favor the emergence of cyclones. All these suggestions will have to be further investigated in the future.

[17] In summary, this study provides a first assessment of the global distribution of upper ocean polarity from drifters, covering scales from large eddies to submesoscale structures. As such, it is complementary to studies based on altimeter data [*Chelton et al.*, 2007], characterized by more homogeneous coverage but with less spatial resolution – of particular importance when examining submesoscale motion. Drifters, on the other hand, might preferentially sample frontal convergence regions, therefore favoring observations of small-scale vortices. The two data sets are highly complementary and we expect that their combined use will help us achieve a more complete view of ocean dynamics.

[18] **Acknowledgments.** Helpful comments by T. Ozgokmen, S. Elipot, D. Chelton, G. Gasparini and M. Lankhorst are gratefully acknowledged. A. G. was partially supported by CNR (Italy) and M. V. by UCSC. R. L. was supported by NOAA Office of Climate Observations and the Atlantic Oceanographic and Meteorological Laboratory. The findings and conclusions in this report are those of the authors and do not necessarily represent the views of the funding agencies.

References

Boccaletti, G., R. Ferrari, and B. Fox-Kemper (2007), Mixed layer instabilities and restratification, *J. Phys. Oceanogr.*, *37*(9), 2228–2250.

Borgas, M. S., T. K. Flesch, and B. L. Sawford (1997), Turbulent dispersion with broken reflectional symmetry, *J. Fluid Mech.*, *279*, 69–99.

Chelton, D. B., R. A. de Szoeke, M. G. Schlax, K. El Naggar, and N. Siwertz (1998), Geographical variability of the first-baroclinic Rossby radius of deformation, *J. Phys. Oceanogr.*, *28*, 433–460.

Chelton, D. B., M. G. Schlax, R. M. Samelson, and R. A. de Szoeke (2007), Global observations of large oceanic eddies, *Geophys. Res. Lett.*, *24*, L15606, doi:10.1029/2007GL030812.

Doglioli, A. M., M. Veneziani, B. Blanke, S. Speich, and A. Griffa (2006), A Lagrangian analysis of the Indian-Atlantic interocean exchange in a regional model, *Geophys. Res. Lett.*, *33*, L14611, doi:10.1029/2006GL026498.

Elipot, S. K. Y. (2006), Spectral characterization of Ekman velocities in the Southern Ocean based on surface trajectories, Ph.D. dissertation, Scripps Inst. of Oceanogr., Univ. of Calif., San Diego. Available at http://repositories.cdlib.org/sio/techreport/49/

Flierl, G. R. (1981), Particle motion in large-amplitude wave fields, *Geophys. Astrophys. Fluid Dyn.*, *18*, 39–74.

Hoskins, B. J., and F. P. Bretherton (1972), Atmospheric frontogenesis models: Mathematical formulation and solution, *J. Atmos. Sci.*, *29*, 11–37.

Lumpkin, R., and Z. Garraffo (2005), Evaluating the decomposition of tropical Atlantic drifter observations, *J. Atmos. Oceanic Technol.*, *22*, 1415–1422.

Munk, W., L. Armi, K. Fischer, and F. Zachariasen (2000), Spirals on the sea, *Proc. R. Soc. London, Ser. A*, *456*, 1217–1280.

Olson, D. B. (1991), Rings in the ocean, *Annu. Rev. Earth Planet. Sci.*, *19*, 283–311.

Richardson, P. L. (1993), A census of eddies observed in North Atlantic SOFAR float data, *Prog. Oceanogr.*, *31*, 1–50.

Rio, M.-H., and F. Hernandez (2003), High-frequency response of wind-driven currents measured by drifting buoys and altimetry over the world ocean, *J. Geophys. Res.*, *108*(C8), 3283, doi:10.1029/2002JC001655.

Rudnick, D. L. (2001), On the skewness of vorticity in the upper ocean, *Geophys. Res. Lett.*, *28*(10), 2045–2048.

Sato, K., T. Suga, and K. Hanawa (2006), Barrier layers in the subtropical gyres of the world's oceans, *Geophys. Res. Lett.*, *33*, L08603, doi:10.1029/2005GL025631.

Sybrandy, A. L., and P. P. Niiler (1991), WOCE/TOGA Lagrangian drifter construction manual, *WOCE Rep. 63*, 58 pp., Scripps Inst. of Oceanogr., La Jolla, Calif.

Tomczak, M., L. Pender, and S. Liefrink (2004), Variability of the subtropical front in the Indian Ocean south of Australia, *Ocean Dyn.*, *54*, 506–519.

Veneziani, M., A. Griffa, A. M. Reynolds, and A. J. Mariano (2004), Oceanic turbulence and stochastic models from subsurface Lagrangian data for the Northwest Atlantic Ocean, *J. Phys. Oceanogr.*, *34*, 1884–1906.

Veneziani, M., A. Griffa, Z. D. Garraffo, and E. P. Chassignet (2005a), Lagrangian spin parameter and coherent structures from trajectories released in a high-resolution ocean model, *J. Mar. Res.*, *63*, 753–788.

Veneziani, M., A. Griffa, A. M. Reynolds, Z. D. Garraffo, and E. P. Chassignet (2005b), Parameterization of Lagrangian spin statistics and particle dispersion in the presence of coherent vortices, *J. Mar. Res.*, *63*, 1057–1083.

A. Griffa, Istituto de Scienze Marine, Consiglio Nazionale delle Ricerche, Forte Santa Teresa, Pozzuolo di Lerici (SP), 19036, Italy. (agriffa@rsmas.miami.edu)

R. Lumpkin, Physical Oceanography Division, NOAA Atlantic Oceanographic and Meteorological Laboratory, 4301 Rickenbacker Causeway, Miami, FL 33149, USA. (rick.lumpkin@noaa.gov)

M. Veneziani, Ocean Sciences Department, University of California, Santa Cruz, Earth and Marine Sciences Building, A-316 Mailroom, Santa Cruz, CA 95064, USA. (milena@ucsc.edu)